



# A role for the ciliary marginal zone in the melanopsin-dependent intrinsic pupillary light reflex<sup>☆</sup>



Ma'ayan Semo, Carlos Gias, Ahmad Ahmado, Anthony Vugler\*

Department of Ocular Biology and Therapeutics, UCL-Institute of Ophthalmology, 11-43 Bath Street, London EC1V9EL, UK

## ARTICLE INFO

### Article history:

Received 1 October 2013

Accepted in revised form 20 November 2013

Available online 5 December 2013

### Keywords:

melanopsin  
ipRGC  
atropine  
iris  
ciliary body  
stem cells

## ABSTRACT

Maintenance of pupillary constriction in light-adapted rodents has traditionally been thought to involve a reflex between retina, brain and iris, with recent work identifying the melanopsin-expressing intrinsically photosensitive retinal ganglion cells (ipRGCs) as the major conduits for retinal input to the brain. There is also a less well-understood phenomenon whereby the iris of some mammals, including mice, will constrict to light when either the eye, or the iris itself is physically isolated from the brain. The intrinsic pupillary light reflex (iPLR) is the term given to pupil constriction in the absence of retinal input to the brain. Here, using an intraocular axotomy approach, we show that the iPLR in conscious mice spans a dynamic range over 3 log units of irradiance. This iPLR response is absent in melanopsin knockout (MKO) mice and can be significantly inhibited by atropine. Immunohistochemistry for cfos and melanopsin, in combination with light exposure revealed a population of small ipRGCs in the retinal ciliary marginal zone (CMZ), which remain responsive to light in axotomised mice. We report that damage to the CMZ in a novel *in vitro* preparation removes a significant component of the iPLR response, while a detailed immunohistochemical analysis of the CMZ in wildtype mice revealed a melanopsin-rich plexus, which was consistently most intense in nasal retina. There were clear examples of melanopsin-positive, direct retino-ciliary projections, which appear to emanate from Brn3b negative, M1 type ipRGCs. These cells are clustered along the melanopsin-rich plexus nasally and may channel ipRGC signals from retina into the iris via ciliary body. Comparison between wildtype and MKO mice reveals that the ciliary body is also weakly stained for melanopsin. Our results show that the full extent of iPLR in mice requires cholinergic neurotransmission and intact signalling at the CMZ/ciliary body. This response may be mediated to some extent by ipRGCs, which send direct projections from the retina into ciliary body. In addition to the melanopsin-mediated iris sphincter constriction suggested by others, we propose a new mechanism, which may involve constriction of the ciliary body and ipRGC-mediated relaxation of the iris dilator muscle.

© 2013 The Authors. Published by Elsevier Ltd. All rights reserved.

## 1. Introduction

In mammals, the pupillary light reflex (PLR) functions to maintain pupil constriction and regulate retinal light exposure during daylight hours. Although the modulation of pupil size involves a complex interaction between cortical, subcortical and autonomic neural circuitry, the PLR in mammals has long been

*Abbreviations:* iPLR, intrinsic pupillary light reflex; ipRGC, intrinsically photosensitive retinal ganglion cell; CMZ, ciliary marginal zone; ChAT, choline acetyl transferase; OPN, olivary pretectal nucleus; MKO, melanopsin knockout.

<sup>☆</sup> This is an open-access article distributed under the terms of the Creative Commons Attribution License, which permits unrestricted use, distribution, and reproduction in any medium, provided the original author and source are credited.

\* Corresponding author. Tel.: +44 (0)2076084064.

E-mail address: [a.vugler@ucl.ac.uk](mailto:a.vugler@ucl.ac.uk) (A. Vugler).

thought to depend upon a relay of irradiance (ambient light) information from retina to the sphincter pupillae muscle of the iris, via the midbrain olivary pretectal nucleus (OPN), Edinger-Westphal nucleus and ciliary ganglion (Alexandridis, 1985).

Our understanding of the neural circuits mediating PLR has advanced significantly over recent years following on from the discovery of a new class of non-rod, non-cone photoreceptors in the mammalian retina (Freedman et al., 1999; Lucas et al., 2001). These are intrinsically photosensitive retinal ganglion cells (ipRGCs) that express the photopigment melanopsin and project to non-image forming brain structures including the OPN (Berson et al., 2002; Hattar et al., 2002; Provencio et al., 2002). A comparison of the PLR in conscious mice lacking either rods and cones or the melanopsin gene has shown that melanopsin signalling accounts for pupillary constriction at higher irradiances (Lucas et al., 2003). Furthermore, the genetic ablation of ipRGCs early in development

not only reduces pupillary constriction to the brightest light, but also eliminates the PLR at low irradiance (Guler et al., 2008).

The ipRGC population in rodents is heterogeneous, with at least 5 different cell classes varying in soma size, morphology, electrophysiological properties and the expression of melanopsin/the POU domain transcription factor Brn3b (Chen et al., 2011; Ecker et al., 2010; Schmidt et al., 2011). In terms of the ipRGC contribution to PLR circuitry, the most recent study in mice lacking Brn3b expressing ipRGCs suggests that this subtype may be particularly important for channelling rod/cone signals into the PLR (Chen et al., 2011).

In addition to the classical PLR pathway outlined above, it has long been known that irises from fish and amphibians (Barr and Alpern, 1963; Seliger, 1962), birds (Tu et al., 2004) and some mammals (Bito and Turansky, 1975; Lau et al., 1992) will constrict in response to light when physically isolated from the retina. Most recently, unilateral intraorbital optic nerve section has been used to isolate this intrinsic PLR (iPLR) in anaesthetised mice, where it was found to be melanopsin dependent (Xue et al., 2011). This study also identified light-induced tension responses in iris sphincter muscles isolated from a wide range of nocturnal/crepuscular mammals. Based on their observation that melanopsin is expressed in the mouse iris, Xue and colleagues proposed that the iPLR is driven by melanopsin signalling in the sphincter muscle.

We have previously reported the existence of a distinctive plexus of melanopsin positive fibres at the edge of the rat retina (Vugler et al., 2008). Given the close proximity of these fibres to the ciliary body (a structure known to provide physical continuity between retina and iris (Smith et al., 2002)), the intriguing possibility exists that some component of the iPLR may derive from melanopsin signalling at the ciliary marginal zone (CMZ) of the retina.

Given that very little is understood about iPLR in mice and that this response is likely to help sustain pupillary constriction during daylight hours in these mammals, the aim of the current study was to investigate this phenomenon further in conscious mice, which had previously undergone intraocular axotomy. The potential contribution of CMZ melanopsin signalling to the mouse iPLR was investigated using functional anatomy in axotomised animals and immunohistochemistry/a novel *in vitro* preparation in un-operated wildtype mice.

## 2. Material and methods

### 2.1. Animals

All procedures were conducted according to the Home Office (UK) regulations, under the Animals (Scientific Procedures) Act of 1986, with local (UCL-Institute of Ophthalmology, London, UK) ethics committee approval and in accordance with EU directive 2010/63/EU. All animals were housed under a 12:12 light dark cycle, with food and water available *ad libitum*. Two strains of mice were used here: wildtype mice of the C3H/He strain and melanopsin knockout (MKO) mice on a C57 BL6/129 mixed strain background (*Opn4<sup>-/-</sup>*, Lucas et al., 2003). The C3H/He mouse was chosen here in order to be consistent with the original studies of melanopsin contribution to the consensual PLR, which also used this strain (Lucas et al., 2001, 2003).

### 2.2. Bilateral intraocular axotomy procedure

A total of 6 wildtype mice (aged 92–348 days) and 5 MKO mice (aged 168–217 days) underwent bilateral intraocular axotomy. Compared to intraorbital axotomy and optic nerve crush techniques which involve dissection through extraocular tissue to access the optic nerve, our intraocular axotomy approach avoids potential

damage to the ciliary ganglion/nerves which run along the optic nerve in mice (Kuder, 1986; Nowak et al., 2004). The intraocular axotomy procedure has been described in detail previously (Semo et al., 2010). Briefly, animals were deeply anaesthetized with a mixture of medetomidine hydrochloride (1 mg/kg) (Domitor, Pfizer, Kent, UK) and ketamine (75 mg/kg) and placed securely in a nose bar with eyes covered in ViscoTears (Novartis Pharmaceuticals UK Ltd). To perform the axotomy, a 30-gauge needle (attached to a 2.5 µl Hamilton syringe) was inserted through the sclera, directly into the sub-retinal space. Once the needle is sub-retinal and adjacent to the optic nerve head, the optic nerve (together with the central retinal artery) was easily severed using a swift back and forth movement. This surgical procedure is summarised in Fig. 1A (adapted from (May and Lutjen-Drecoll, 2002)). Following bilateral axotomy surgery, all animals were given an intra-peritoneal injection of the analgesic carprofen 5 mg/kg (Rimadyl, Pfizer, Kent, UK) and recovered with the anaesthetic antidote atipamezole 0.5 mg/kg (Anti-sedan Pfizer, Kent, UK).

### 2.3. *In vivo* pupillometry

The iPLR was assessed *in vivo* using pupillometry in conscious mice that had been dark-adapted overnight before testing. The iPLR recordings were completed 2 months following bilateral axotomy, with pupillometry performed between the hours of 9:00–11:00 in order to control for any circadian variation in the response.

The apparatus and protocol for recording the PLR in unanaesthetised mice has been described in detail previously (Semo et al., 2010) and is illustrated in Fig. 1B. Briefly, the left eye was illuminated with an infra-red light source and stimulated with broad-spectrum light originating from a xenon-arc lamp (Lambda DG-4, Linton Instrumentation). The stimulating light was heat filtered (preventing the passage of wavelengths >600 nm) then guided with a fibre optic 1 cm away from the left eye stimulating with white light at irradiances of either 63, 6.3, 0.63 or 0.063 mW/cm<sup>2</sup>, produced using appropriate neutral density filters. The iPLR response was measured in each animal using all 4 irradiances (presented on separate days) whilst the consensual response was measured only at the highest irradiance (63 mW/cm<sup>2</sup>). For the consensual response the light was guided directly to the stimulated (left) eye by a 1 cm cone of black cardboard fixed to the end of the fibre optic, surrounding the eye completely and preventing stray light from reaching the recorded (right) eye. For all PLR recordings, frames were collected for 75 s, with 5 s of baseline prior to stimulation for 60 s. The pupil area was measured off-line at 1 s intervals by an observer using bespoke MATLAB software. PLR measurements are expressed as normalised pupil area (relative to baseline pupil area).

Upon completion of all 5 pupillometry tests, the wildtype mice were dark-adapted overnight again and the iPLR was measured following atropine application. Under dim red light illumination animals had 1 drop of atropine sulphate, 1%, (Minims, preservative free) applied to their left eye. They were returned to the dark for 30 min prior to eliciting the iPLR with 63 mW/cm<sup>2</sup> bright white light (5 s baseline plus 60 s stimulation).

### 2.4. Functional anatomy using immunohistochemistry for *cfos* in axotomised mice

At 2 months post-surgery, following the completion of iPLR recordings, all wildtype axotomised animals were dark-adapted overnight and then either exposed to room lighting (0.2 mW/cm<sup>2</sup> white light) for 90 min ( $n = 3$ ) or remained in darkness ( $n = 3$ ) prior to perfusion. Animals were then deeply anaesthetised with sodium pentobarbital (60 mg/kg) and perfused (in a counterbalanced

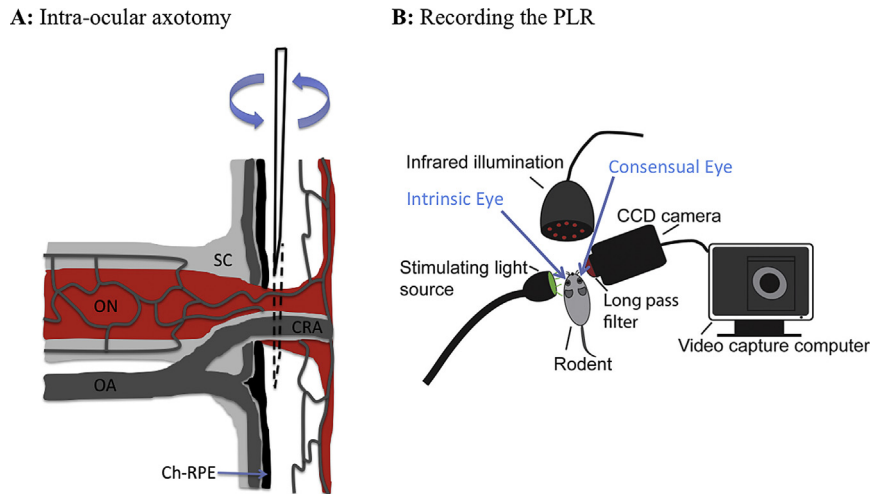


**Fig. 1.** Schematics of the intraocular axotomy procedure (A. adapted from [May and Lutjen-Drecoll, 2002](#)) and the apparatus used to record iPLR responses (B).

fashion) with 0.1 M PBS followed by 4% paraformaldehyde (in 0.1 M phosphate buffer). The left eye from each animal was post-fixed for 2 h prior to removal of the retina and vitreous using a previously described technique ([Vugler et al., 2008](#)). Entire retinal whole mounts were impossible to obtain from these mice due to an absence of central retina. Instead, small retinal fragments were washed in 0.1 M PBS and processed for *cfos* and melanopsin double labelling at room temperature as follows: Incubation for 2 h in a blocking solution containing 5% normal donkey serum (NDS) in 0.1 M PBS with 3% Triton X-100, followed by overnight incubation with rabbit anti-Fos (1:5000, PC38 Merck Millipore, Darmstadt, Germany) diluted in 0.1 M PBS containing 1% NDS and 3% Triton. The following day, retinal segments were washed in PBS and incubated for 2 h in FITC-labelled donkey anti-rabbit secondary antibody (Jackson ImmunoResearch, West Grove, PA) diluted 1:200 in 0.1 M PBS containing 2% NDS and 0.3% Triton. The segments were then washed extensively prior to overnight application of rabbit anti-melanopsin (1:5000, UF006 Advanced Targeting Systems, San Diego, US) in 0.1 M PBS with 1% NDS. The following day, retinal segments were washed in PBS and incubated for 2 h in TRITC-labelled donkey anti-rabbit secondary antibody (Jackson ImmunoResearch) diluted 1:200 in 0.1 M PBS. This consecutive rabbit antibody labelling technique is a modification of a previous method ([Semo et al., 2003](#)) that allows distinction between Fos staining in yellow and melanopsin staining in red. One retinal segment was processed in the absence of primary antibodies as a negative control.

Following perfusion, the right eye from each animal was post-fixed overnight at 4 °C, cryoprotected with 30% sucrose (in 0.1 M PBS) overnight at 4 °C, lens removed and frozen in OCT embedding compound. Sections were then taken through the central region of each eye (14 μm thick) and mounted onto Superfrost Plus slides (BDH). They were then double-labelled with the rabbit anti-melanopsin antibody (1:5000) and goat anti-calretinin (1:5000, Swant, Bellinzona, Switzerland) and visualised with the appropriate secondary antibody using a previously described protocol ([Vugler et al., 2008](#)). Calretinin normally stains retinal ganglion cell axons leaving the retina via the optic nerve and as such is a useful marker to confirm intraocular axotomy ([Semo et al., 2010](#); [Vugler and Coffey, 2003](#)). Immunohistochemical staining was analysed using a Zeiss LSM 510 confocal microscope with associated LSM image browser software. Retinal structure was additionally visualised using nomarski optics under transmitted light. Some

sections were processed in the absence of primary antibodies as a negative control.

#### 2.5. Immunohistochemistry on retinal whole mounts from un-operated mice

Retinal whole mounts were obtained from wildtype ( $n = 5$  animals) and MKO ( $n = 3$  animals) mice using our previously described method ([Vugler et al., 2008](#)). Briefly, animals were perfused as detailed above and both eyes were post-fixed for 2 h prior to careful orientation of retinae using 1 large dorsal cut and three smaller cuts in nasal, temporal and ventral retina. The CMZ region was removed in its entirety along with the ciliary body (which was physically attached to the retina) by gradually sliding a pair of closed microsurgical tweezers under the retinal periphery. Vitreous was removed with filter paper and retinae were double labelled with the rabbit anti-melanopsin antibody (1:5000) in combination with either goat anti-ChAT (anti-Choline acetyl transferase, 1:250, AB144P, Millipore) or goat anti-Brn3b (1:100, Santa Cruz Biotechnology, Santa Cruz, US). The anti-ChAT antibody was applied in order to delineate the edge of the neural retina and the anti-Brn3b antibody was applied in order to distinguish between the Brn3b negative M1 type ipRGCs and the other subclasses of ipRGCs that express this transcription factor ([Schmidt et al., 2011](#)). The primary antibodies were visualised using TRITC-labelled donkey anti-rabbit (1:200, Jackson ImmunoResearch) and FITC-labelled donkey anti-goat (1:200, Jackson ImmunoResearch) antibodies and the whole mounts were mounted/coverslipped as previously described ([Vugler et al., 2008](#)). Immunohistochemical staining was analysed using a Zeiss LSM 510 confocal microscope with associated LSM image browser software. Retinal structure was additionally visualised using nomarski optics under transmitted light. One representative wildtype retina was imaged in its entirety using a Zeiss LSM 710 confocal microscope equipped with intelligent tiling software. One wildtype retina was processed in the absence of primary antibodies as a negative control.

#### 2.6. *In vitro* pupillometry on anterior eye chamber preparations

The apparatus used for recording *in vitro* pupillometry was identical to that described in Section 2.3 above, with all recordings made in response to stimulation at the brightest irradiance (63 mW/cm<sup>2</sup>). Wildtype mice (216–314 days old,  $n = 9$  animals)

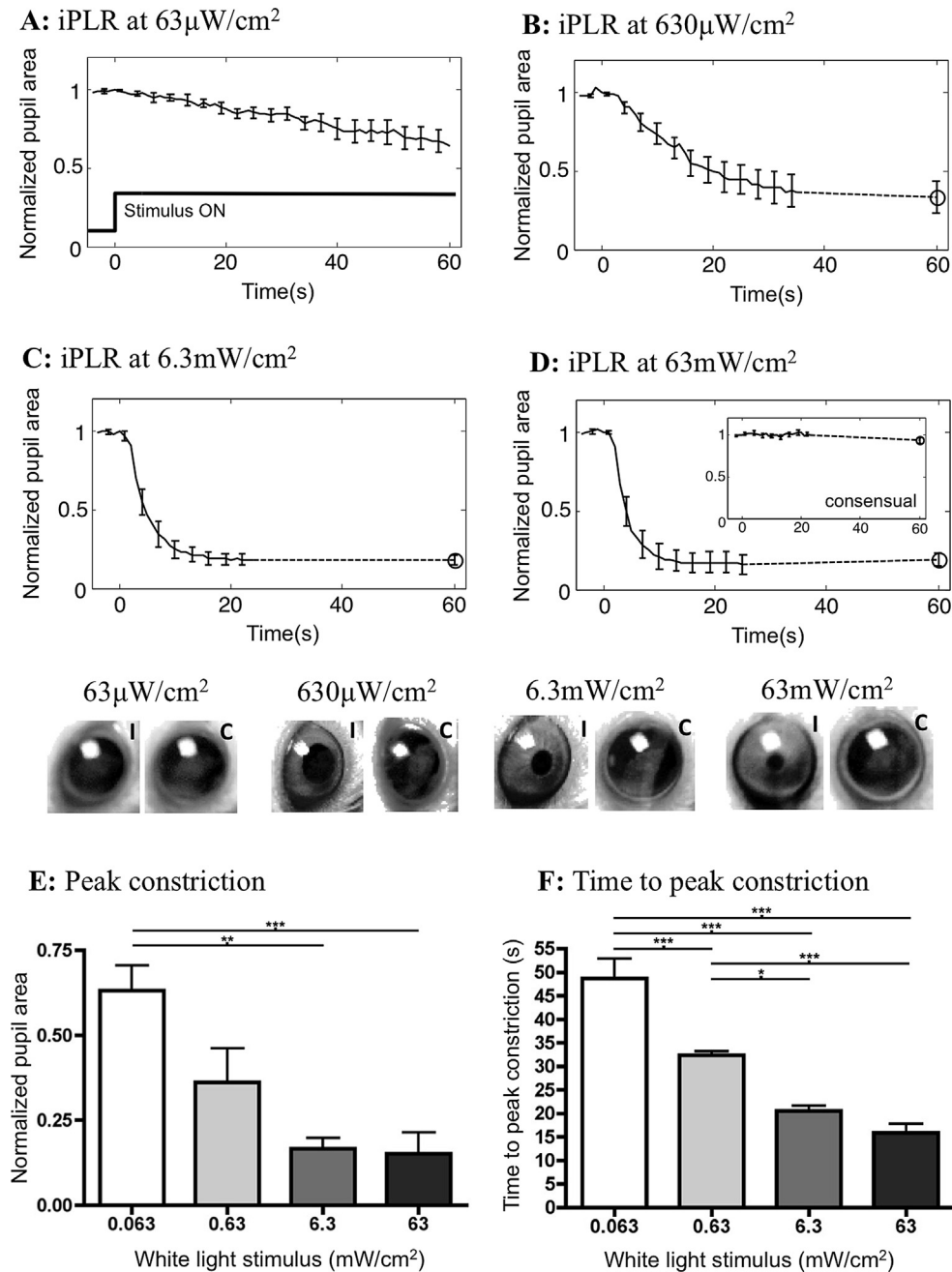


**Fig. 2.** Intraocular axotomy isolates the iPLR in conscious wildtype mice. **A–D**, sensitivity of the iPLR to light of increasing irradiance. The graphs show pupil area relative to baseline, where a marked increase in both the speed and strength of the iPLR occur up until  $6.3\text{ mW}/\text{cm}^2$ . No consensual responses could be recorded (inset into **D**). Representative intrinsic (I) and consensual (C) pupil images (taken at 20 s post-stimulation) are shown for each irradiance below graphs A–D. The graph in **E** shows how the peak constriction achieved in wildtype mice increases at irradiances up to  $6.3\text{ mW}/\text{cm}^2$ . The graph in **F** shows how latency of constriction reduces with increasing irradiance. All values plotted indicate the mean  $\pm$  SEM with stars (\*) indicating significance levels (*post hoc* Bonferroni's multiple comparison tests): \* $P < 0.05$ ; \*\* $P < 0.01$ ; \*\*\* $P < 0.001$ .

were dark-adapted overnight prior to the anterior eye chamber experiment, which was performed between 08:00–11:00 and consisted of two experimental groups: 1. Eyes in which the anterior chamber was removed by cutting immediately below the border between cornea and sclera to cause damage at the CMZ (CMZ-cut), 2. Eyes in which the anterior chamber was removed by cutting more posteriorly into the sclera, approximately 1 mm below the cornea (retina-cut). Our use of the CMZ cut was based on pilot histology work indicating that cuts made along the pigmented transition between cornea and sclera are effective in minimising retinal inclusion in anterior eye chamber preparations.

On the morning of experimentation, dark-adapted mice were killed swiftly by cervical dislocation under red illumination. The anterior chamber was then removed under bright red illumination while the eye remained *in situ* by making an incision at the desired level of the eye with a microsurgical blade and then cutting around the eye at this level with a pair of microsurgical scissors. The anterior chamber (plus lens) was then carefully placed on a custom made Perspex indentation to hold it upright and covered with 3 drops of Neurobasal<sup>®</sup> culture medium (Invitrogen, 12348-017), which had been preheated to  $37\text{ }^\circ\text{C}$ . The iPLR was recorded from the isolated anterior chamber by placing its anterior surface 1 cm from

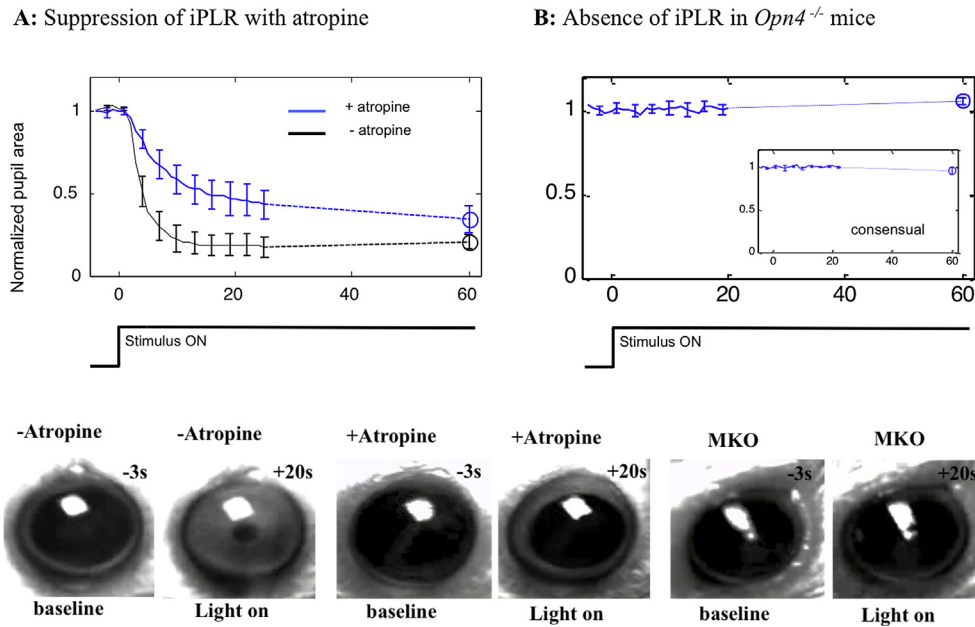


**Fig. 3.** The iPLR depends upon melanopsin and is facilitated by cholinergic neurotransmission. As shown in **A**, atropine application significantly reduces the speed and amplitude of the iPLR. **B**, the iPLR was absent in MKO mice, which also failed to exhibit a consensual PLR response (**B**, inset). Representative pictures from baseline (3 s before light onset (-3)) and light on (20 s post-stimulation (+20)) are shown below the graphs.

the stimulating fiber optic light source, with 30 s of baseline recording followed by 60 s of light stimulation and a further 60 s of post-stimulation recording. The left and right eyes from each mouse were prepared by CMZ cut or retinal cut in a counter-balanced fashion and recordings were completed from both eyes of one mouse in less than 15 min (approximately 5 min from death until the first recording started). Acetylcholine hydrochloride (28 mM, Sigma) was added to the CMZ-cut preparations after recordings had been made in order to test the ability of these anterior chambers to undergo full pupillary constriction. The pupil area was measured off-line at 1 s intervals by an observer using the bespoke MATLAB software. PLR measurements are expressed as normalised pupil area (relative to baseline pupil area). Following experimentation the anterior segments were fixed in 4% paraformaldehyde, cryoprotected and sectioned (14  $\mu\text{m}$  thick) prior to counterstaining with DAPI, cover slipping and imaging using a Zeiss LSM 700 confocal microscope.

### 2.7. Statistical analysis

All data was analysed using GraphPad Prism software (GraphPad Software, San Diego, CA). Comparisons of pupil constriction were made using two-way repeated measures ANOVA followed by Bonferroni *post hoc* tests. Peak constriction levels and latencies were analysed using one-way ANOVA followed by Bonferroni's multiple comparison tests or one-tailed *t*-tests.

## 3. Results

### 3.1. In vivo sensitivity of the iPLR

We tested the sensitivity of the iPLR in conscious mice using a bright white light (Fig. 2A–D) at intensities ranging from 0.063 to 63  $\text{mW}/\text{cm}^2$  increasing in log unit steps. This is approximately equivalent (at 480 nm) to  $1 \times 10^{14}$ ,  $10^{15}$ ,  $10^{16}$ ,  $10^{17}$  photons/ $\text{cm}^2/\text{s}$  at the cornea, which equates to the higher operating range for the melanopsin photopigment in the consensual PLR (Lucas et al.,

2003) and is very similar to the sensitivity range reported for iPLR in anaesthetised mice (Xue et al., 2011). All wildtype mice were confirmed as axotomised by the lack of consensual PLR elicited by stimulating the intrinsic eye with the brightest light intensity (Fig. 2D inset). Additionally, MKO mice axotomised using the same method also lacked both the consensual and intrinsic PLR (Fig. 3B). This finding suggests that autonomic activity alone does not cause pupillary constriction in our conscious preparation and is in agreement with the study by Xue et al. (2011) which showed a requirement for melanopsin in the production of iPLR.

As shown in Fig. 2, increasing the light intensity clearly alters the kinetics of the iPLR, with slower rates of constriction and smaller constrictions (larger pupil area) at the lower light intensities compared to the higher ones. Two-way repeated measures ANOVA reveals that there is a significant effect of time  $P < 0.0001$  ( $F_{27,540} = 189.72$ ), light intensity  $P < 0.0001$  ( $F_{3,540} = 31.25$ ) and an interaction between the two factors  $P < 0.0001$  ( $F_{81,540} = 22.36$ ), subjects were significantly matched  $P < 0.0001$  ( $F_{20,540} = 50.54$ ). Bonferroni post test results (analysed up to 23 s post light pulse) show: Between 0.063 and 0.63  $\text{mW}/\text{cm}^2$  (Fig. 2A and B) the peak constriction is significantly greater at the higher intensity between 12 s and 23 s post light pulse. Between 0.63 and 6.3  $\text{mW}/\text{cm}^2$  (Fig. 2B and C) the peak constriction is again significantly greater at the higher light intensity between 3 and 23 s post light stimulus. However, between 6.3 and 63  $\text{mW}/\text{cm}^2$  (Fig. 2C and D), Bonferroni post tests do not detect differences in the pupil area attained.

The peak pupil constriction attained during stimulation (Fig. 2E) was significantly enhanced by increasing light intensity (one-way ANOVA,  $P = 0.0003$  ( $F_{3,23} = 9.880$ )) and Bonferroni's multiple comparison tests revealed a significantly reduced pupil area attained at 6.3 versus 0.063  $\text{mW}/\text{cm}^2$  ( $P < 0.01$ , pupil area reduced by ~47%) and 63 versus 0.063  $\text{mW}/\text{cm}^2$  ( $P < 0.001$ , pupil area reduced by ~48%). However, although the most constricted pupils were observed following 63  $\text{mW}/\text{cm}^2$ , the normalised pupil area does not get significantly smaller between the two highest light intensities (6.3 versus 63  $\text{mW}/\text{cm}^2$ , pupil area reduced by ~1.5% between these two intensities).

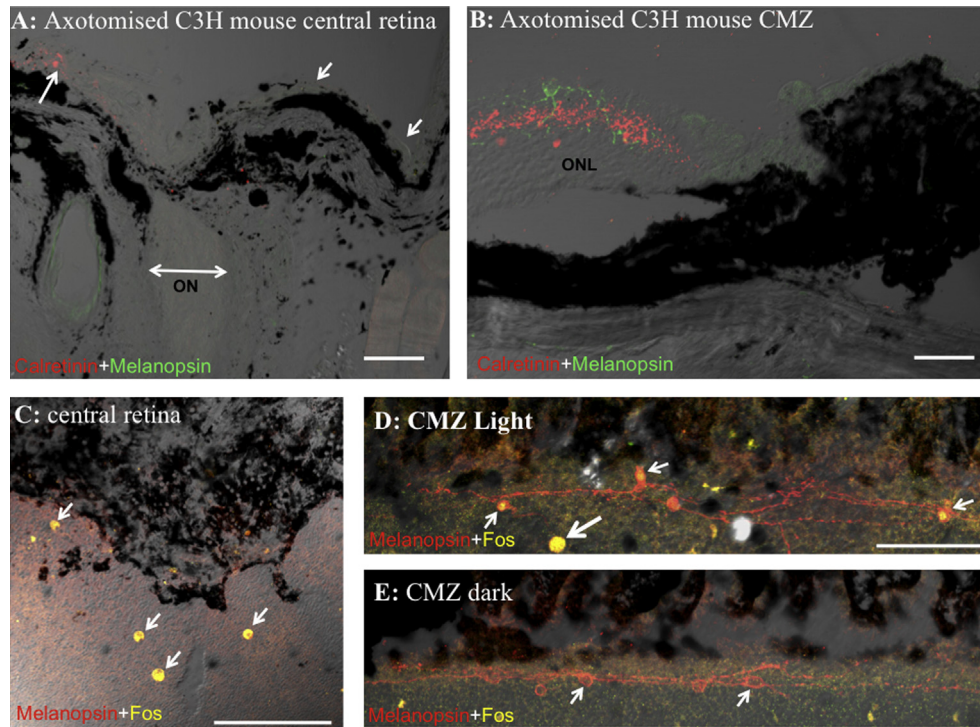


**Fig. 4.** Functional anatomy reveals ipRGC light responses in the CMZ of bilaterally axotomised wildtype mice. **A**, sections through the right eye revealed severe atrophy of central retina (small arrows), with some residual staining for calretinin (large arrow) which did not extend into the optic nerve (ON, double arrow). **B**, surviving melanopsin cells (green) were found in the CMZ of the same eye. Whole mount fragments, processed for functional anatomy (**C**) revealed an absence of central retina/melanopsin staining, with retinal pigment epithelial scar tissue and associated autofluorescent macrophages (arrows). **D–E**, images from the CMZ showing small melanopsin positive ipRGCs (red, arrows), which localise nuclear Fos (yellow) in response to light (small arrows in **D**) but not in dark control mice (arrows in **E**). The large arrow in **D** points to an autofluorescent macrophage. Images shown are representative of the left and right eyes from the three light-exposed and 3 dark-control mice used in this experiment. Scale bars: **A**, 100  $\mu\text{m}$ ; **B**, 50  $\mu\text{m}$ ; **C**, 200  $\mu\text{m}$ ; **D–E**, 100  $\mu\text{m}$ . (For interpretation of the references to colour in this figure legend, the reader is referred to the web version of this article.)

As shown in Fig. 2F, the latency of iPLR also changes significantly between the different light intensities, with the time to peak constriction being significantly delayed at lower light levels (one-way ANOVA  $P < 0.0001$  ( $F_{3,23} = 35.68$ )). Bonferroni's multiple comparison test also revealed significantly decreased time to peak at each increment of higher light intensity up until 6.3  $\text{mW}/\text{cm}^2$  (0.063 versus 0.63  $\text{mW}/\text{cm}^2$   $P < 0.001$ , and 0.63 versus 6.3  $\text{mW}/\text{cm}^2$   $P < 0.05$ ). Despite a shorter mean latency at 63  $\text{mW}/\text{cm}^2$  ( $\sim 20\%$  reduction) there was no significant difference between the two highest light intensities.

These results suggest that there is a dynamic range in the *in vivo* iPLR of around 3 log units between  $\sim 10^{14}$ – $10^{16}$  photons/ $\text{cm}^2/\text{s}$  (equivalent at 480 nm) with the response becoming asymptotic between  $\sim 10^{16}$  and the extremely high light level of  $\sim 10^{17}$  photons/ $\text{cm}^2/\text{s}$ .

### 3.2. Atropine application inhibits the iPLR

As shown in Fig. 3A, although the *in vivo* iPLR was resistant to atropine application, it was not entirely unaffected by it. Two-way repeated measures ANOVA revealed a significant effect of time  $P < 0.0001$  ( $F_{28,280} = 112.3$ ), and atropine  $P < 0.05$  ( $F_{1,280} = 8.168$ ) and an interaction between the two factors  $P < 0.0001$  ( $F_{28,280} = 7.838$ ), subjects are significantly matching  $P < 0.0001$  ( $F_{10,280} = 80.99$ ).

Furthermore, Bonferroni *post hoc* tests reveal that the peak level of pupil constriction is significantly lower in the atropine treated compared to the untreated 4–15 s post stimulus onset. The peak constriction attained (in the first 24 s post-stimulus) is also significantly greater in the untreated compared to atropine treated ( $t$ -test  $P < 0.05$ , untreated 0.15 (normalized pupil area)  $\pm 0.06$  (SEM)

versus atropine treated 0.44 (normalized pupil area)  $\pm 0.09$  (SEM)). The iPLR constriction is also slower following atropine application, with time to this peak constriction being significantly delayed in the atropine treated eyes ( $t$ -test  $P < 0.05$ , untreated 15.8 (s)  $\pm 1.92$ (SEM) versus atropine treated 21.3 (s)  $\pm 1.7$ (SEM)). At 60s post-stimulus the atropine treated pupil area although slightly larger ( $\sim 15\%$ ) than the untreated eye, is now statistically indistinguishable from it (one-tailed  $t$ -test  $P > 0.05$ ). Although the pupils of atropine-treated mice sometimes appeared larger at baseline (see images in Fig. 3), we were unable to detect a statistically significant effect of atropine on baseline pupil diameter (data not shown). Our data suggests that the iPLR in conscious mice is strongly facilitated by cholinergic neurotransmission.

### 3.3. Peripheral ipRGCs survive and function in axotomised mice

As shown in Fig. 4, immunohistochemistry on sections and whole mount retinal fragments taken from eyes of the bilaterally axotomised mice revealed widespread destruction to central retina, with an absence of calretinin staining in the optic nerve of all right eyes. Under normal circumstances, calretinin is a robust marker of RGC axons in the rodent optic nerve (Semo et al., 2010; Vugler and Coffey, 2003). Surviving melanopsin positive ipRGCs were only found in the far peripheral retina of both sectioned and whole mount material. Fig. 4 shows representative images from the left and right eyes of the axotomised mice. As can be seen clearly in Fig. 4D–E, exposure to light for 90 min caused nuclear localisation of Fos in a sparse population of small ( $\sim 12$   $\mu\text{m}$  diameter) ipRGCs located in the CMZ. These cells were aligned along a sparse plexus of melanopsin positive fibres and the images in Fig. 4D–E represent the best examples of this structure in the retinal fragments

available to us. Due to the nature of the whole mounted material we were unable to quantify ipRGC survival in peripheral retina, however, all ipRGCs examined in light exposed tissue contained nuclear Fos, while this was absent from all ipRGCs examined in the dark control group. Where fragments including central retina were processed, the neural retina had been replaced by retinal pigment epithelial scar tissue and melanopsin positive cells were absent (Fig. 4C). Autofluorescent macrophages were observed in this region (arrows in Fig. 4C) and are a common feature following surgical trauma to the retina (Hasan et al., 2010). As shown under nomarski optics in Fig. 4B, the outer nuclear layer (ONL) also survived axotomy in the retinal periphery of these mice. There was an absence of immunostaining for melanopsin, calretinin and Fos in the tissue processed with omission of primary antibodies.

#### 3.4. Damage to the CMZ significantly reduces the iPLR in mice

Using our novel *in vitro* anterior eye chamber preparations we found that compared to cuts made in the retina (retina-cut group), cuts made in the vicinity of CMZ (CMZ-cut group) significantly reduced the extent and speed of the iPLR (see Fig. 5A and supplementary video files SV1 and SV2). Two-way repeated measures ANOVA revealed that there was a significant effect of time  $P < 0.0001$  ( $F_{85,1275} = 10.96$ ), cut  $P < 0.05$  ( $F_{1,1275} = 4.653$ ) and an interaction between the two factors  $P < 0.0001$  ( $F_{85,1275} = 2.213$ ), with subjects significantly matching  $P < 0.0001$  ( $F_{15,1275} = 324.1$ ). Time to peak constriction was longer in the CMZ-cut group

compared to retina-cut group ( $t$ -test  $P < 0.05$ , retina-cut  $20.3$  (s)  $\pm 4.9$ (SEM) versus CMZ-cut  $\pm 39.4$  (s)  $\pm 8.3$ (SEM)). The constriction attained was also significantly greater in the retina-cut preparation ( $t$ -test  $P < 0.05$ , retina-cut  $0.52$  (normalized pupil area)  $\pm 0.09$ (SEM) versus CMZ-cut  $0.73$  (normalized pupil area)  $\pm 0.05$ (SEM)). The process of CMZ damage in the CMZ-cut group did not significantly affect the baseline diameter of the pupil (data not shown), nor did it prevent the iris muscles from producing a full pupillary constriction following acetylcholine application (Fig. 5B inset). Histological analysis of the anterior eye chamber preparations revealed consistent damage to the CMZ following CMZ-cut (Fig. 5B) and consistent inclusion of CMZ in the retina-cut group (Fig. 5C). This data suggests that signalling at the CMZ region is required for the production of a full iPLR response in mice.

Supplementary video related to this article can be found at <http://dx.doi.org/10.1016/j.exer.2013.11.013>.

#### 3.5. Retinal ipRGCs extend small processes directly into the ciliary body

Next we focused our attention back on the CMZ region of wildtype mice in order to understand further why damage to this region may inhibit the melanopsin-dependent iPLR response. Immunostaining for melanopsin in carefully dissected wildtype retinal whole mounts revealed a striking plexus of melanopsin fibres running along the CMZ of the retina. As shown at low magnification in Fig. 6A, this plexus was most intense along the

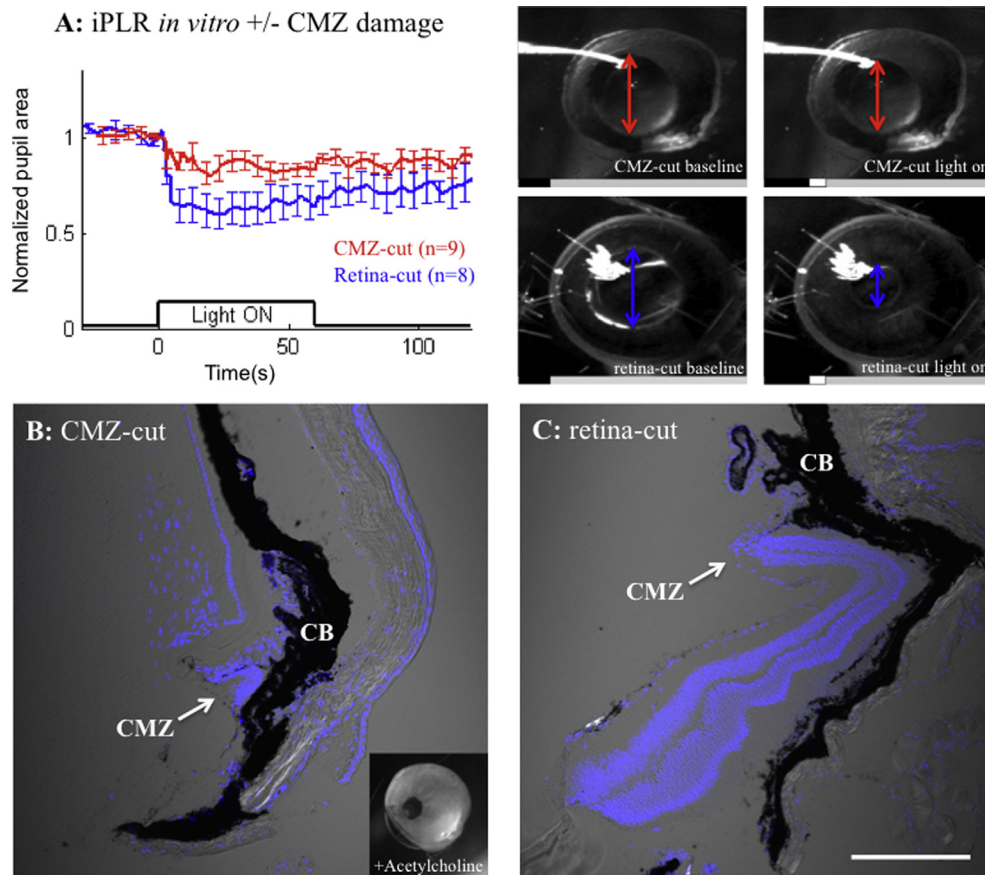


**Fig. 5.** Targeted damage to the CMZ causes a significant reduction in the iPLR response of mice. **A**, graph showing the iPLR in anterior eye cups prepared using either the CMZ-cut or retina-cut method (values indicate mean  $\pm$  SEM). Representative baseline (10 s prior to stimulus onset) and light on (10 s after stimulus onset) video images are shown to the right. **B**, representative histology for the CMZ-cut group showing damage to the CMZ of the retina, which lies adjacent to the ciliary body (CB). Inset image in **B** shows full constriction in the CMZ-cut preparation 8 min following acetylcholine application. **C**, representative histology from the retina-cut group. Scale bar, 200  $\mu$ m.

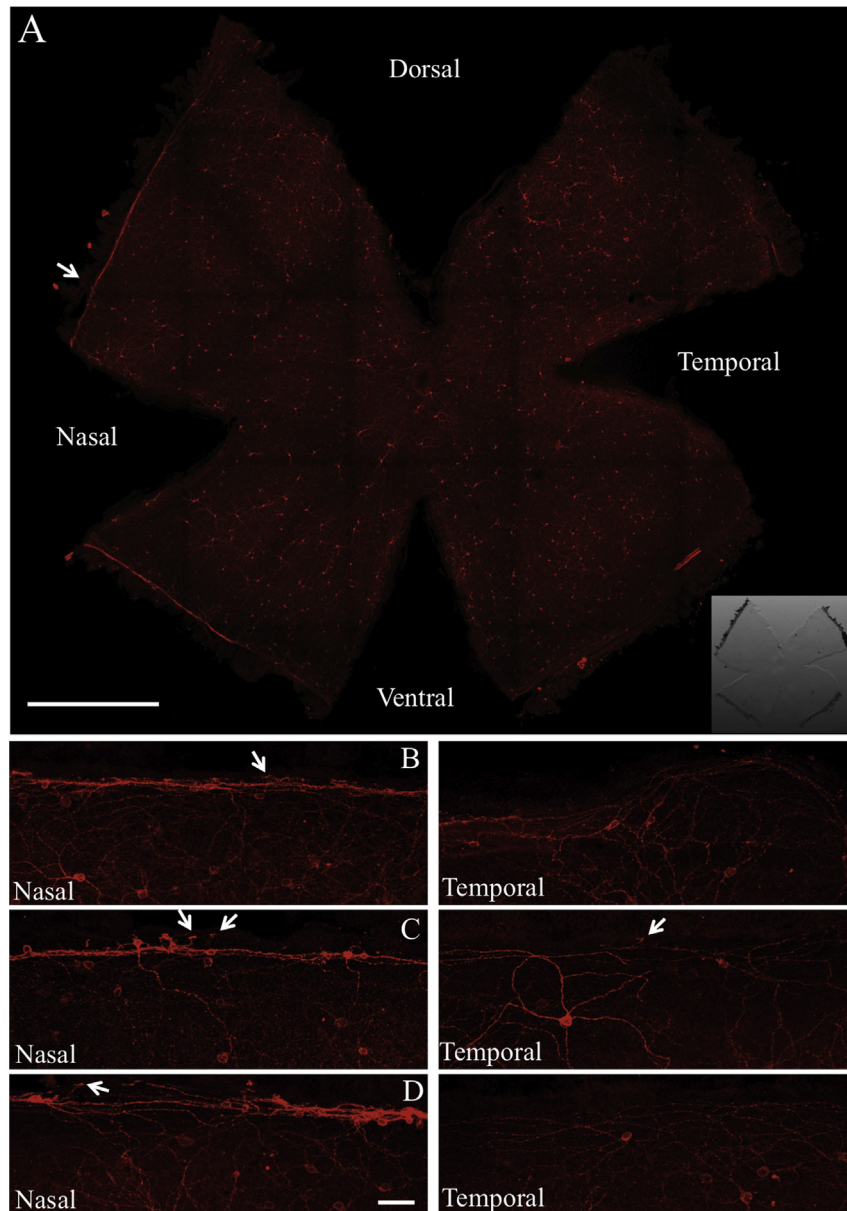


**Fig. 6.** The CMZ of mice contains a plexus of melanopsin-positive processes which is most intense nasally. **A**, low power confocal photomontage of the left retina of a wildtype mouse showing a striking structure towards the far periphery of nasal retina. Inset in **A** shows the same retina viewed under transmitted light. **B–C** shows the nasal and temporal CMZ from three different animals. The arrow in **A** points to the region magnified in **Fig. 7**. Arrows in **B–D** point towards blind-ending melanopsin fibres, which project away from the retinal plexus. Note the occurrence of small melanopsin-positive somas aligned along the nasal but not the temporal plexus. Melanopsin immunoreactivity in red. Scale bars: **A**, 1 mm; **B–D**, 50  $\mu\text{m}$ . (For interpretation of the references to colour in this figure legend, the reader is referred to the web version of this article.)

nasal retinal periphery. While ipRGCs also extended melanopsin positive processes towards the CMZ in temporal retina, the plexus here was far less intense (**Fig. 6B–D**). This melanopsin-rich nasal CMZ structure was found in all 9 wildtype retinæ examined (both left and right from  $n = 5$  mice) and was characterised by numerous small ipRGC somas aligned along its length (mean soma diameter,  $11.7 \mu\text{m} \pm 0.33$  from  $n = 15$  cells).

Counterstaining with ChAT to demarcate the limits of neural retina, together with concurrent confocal imaging on the fluorescence and transmitted light channels revealed that some melanopsin-positive processes extended beyond the neural retina and directly into the pigmented ciliary body, which itself showed low level immunoreactivity for both markers (**Fig. 7**), which was absent from negative control tissue (data not shown). These

melanopsin-positive retino-ciliary projections were blind-ending, rare (5–10 clear examples per retina) and could be observed in both nasal and temporal retina (arrows in **Figs. 6B–D** and **8A–B**). No co-localisation was observed between melanopsin-positive ipRGCs and ChAT.

Comparison between melanopsin immunostaining from wild-type and MKO retinal whole mounts confirmed the presence of low levels of the melanopsin protein in cells of the ciliary body (**Fig. 8D–E**). There were also occasional foci of what appeared to be positive melanopsin staining in more distal regions of the ciliary body, however, similar foci were observed in MKO tissue (arrow in **Fig. 8C**) and are therefore non-specific staining artefacts. Finally, counterstaining with an antibody against Brn3b revealed that the majority of ipRGCs towards the CMZ are negative for this

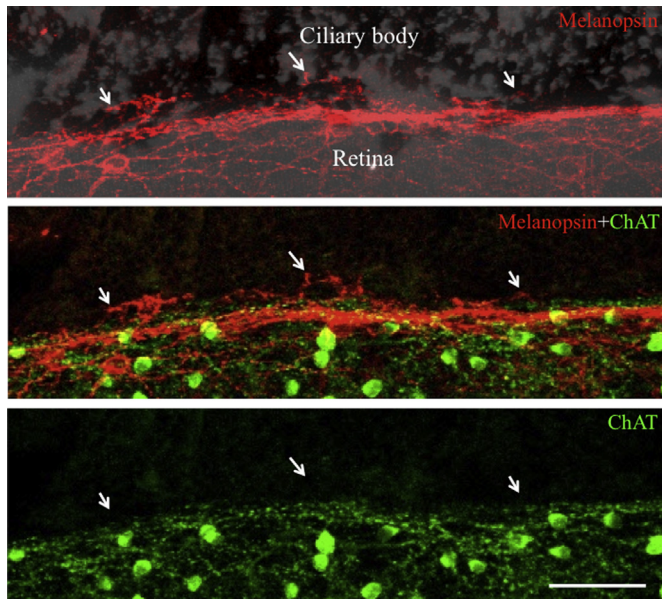


**Fig. 7.** Melanopsin positive retinal-ciliary projections exist in the mouse. High magnification image of the region marked by the arrow in Fig. 6A. The tissue has been stained for melanopsin (red) and ChAT (green) in order to demarcate the boundary of neural retina. The arrows point to melanopsin positive processes that transgress outside of the retina and enter the pigmented ciliary body. Images are from different channels of the same confocal projection. Scale bar: 50  $\mu$ m. (For interpretation of the references to colour in this figure legend, the reader is referred to the web version of this article.)

transcription factor (Fig. 9), a finding that suggests this population of ipRGCs belongs to the Brn3b negative M1 cells described previously (Chen et al., 2011; Schmidt et al., 2011). The intensely fluorescent patches on the green (Brn3b) channel of Fig. 9 are non-specific staining artefact caused by an aggregation of primary antibody on residual vitreous humour (this was not seen in negative control tissue).

#### 4. Discussion

Here, using an intraocular axotomy approach to isolate the iPLR in conscious mice, we report a dynamic range for this response which closely matches that found following intraocular axotomy in anaesthetised mice (Xue et al., 2011). As such, our data supports a role for the iPLR in maintaining pupillary constriction in rodents across a wide range of environmental lighting conditions. We also confirm that the iPLR response is absent in adult mice which lack melanopsin from birth. However, our data does not support the hypothesis put forward by Xue and colleagues that the iPLR is driven solely by melanopsin signalling in the iris sphincter muscle.

When the CMZ was selectively damaged in our anterior eyecup experiment, the iPLR was significantly reduced, with only a residual “twitch” remaining which presumably arose from melanopsin signalling in the iris sphincter muscle. The absence of iPLR in MKO mice, together with comparison between responses in CMZ-cut versus retina-cut preparations strongly suggests that a major component of the iPLR arises from melanopsin signalling in the vicinity of CMZ. Rather excitingly, the results of our *in vivo* atropine experiment and anatomical investigation of wildtype CMZ both implicate neural signalling as a potential contributor to the iPLR response.

Our finding that atropine significantly reduces the magnitude and speed of iPLR *in vivo* was surprising given that previous studies have reported no effect of this muscarinic antagonist on the iPLR response (Barr and Alpern, 1963; Bito and Turansky, 1975; Lau et al.,

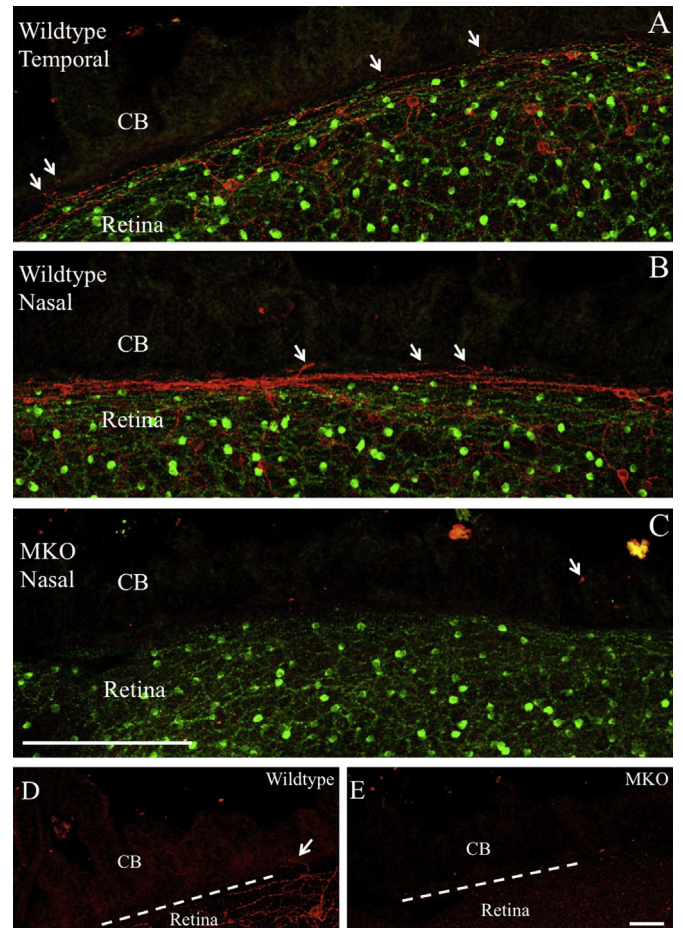


**Fig. 8.** Melanopsin immunoreactivity is absent in the ciliary body (CB) of MKO mice. The arrows in A–B show further examples of blind ending melanopsin fibres, which were absent in MKO mice (C). The arrow in C points to non-specific artefact. The arrow in D points to a melanopsin positive process which projects out of the retina and into the weakly melanopsin-positive ciliary body (compare CB region in D and E). The dashed line in D and E approximates the boundary between neural retina and ciliary body. Scale bars: A–C, 200  $\mu$ m; D–E, 30  $\mu$ m.

1992; Xue et al., 2011). In particular, the study by Lau and colleagues found that the iPLR of axotomised hamsters was resistant to atropine application. This may have been due to damage of the ciliary nerves during their intraorbital axotomy procedure, which would potentially reduce the role of cholinergic neurotransmission in the iPLR. Alternatively, the discrepancy between our atropine data and that from other studies may reflect the intense light used in the current study. Regardless, the effect of atropine we observed was robust and suggests that a significant component of the iPLR involves cholinergic neurotransmission. This may simply result from the indirect release of acetylcholine from parasympathetic nerve terminals following melanopsin-driven muscle contraction in the ciliary body/iris. However, there may also be a role for direct synaptic communication between ipRGC axons and cholinergic terminals in the iris.

Our immunohistochemical investigation of the peripheral mouse retina revealed a striking anatomical structure in the CMZ which is similar to that reported previously in rat (Vugler et al., 2008). This plexus of melanopsin fibres in mice was most intense nasally, with clear examples of melanopsin-positive fibres projecting from ipRGCs at the CMZ directly into the ciliary body. Although the structure we observed previously in rat was least intense in the ventral-temporal retina (Vugler et al., 2008), the melanopsin-CMZ plexus in mouse is more anatomically compartmentalised. We

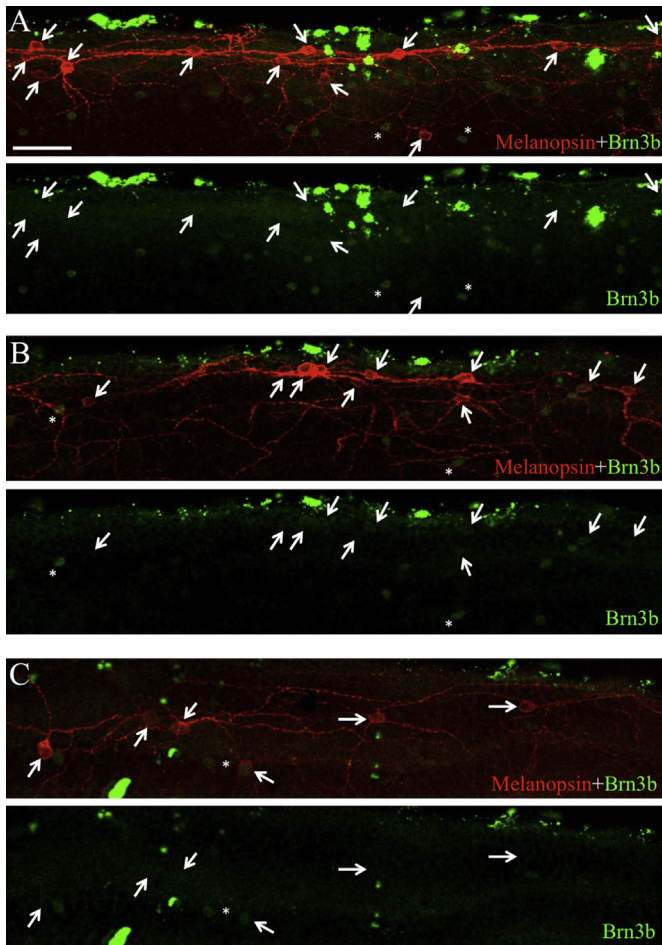


**Fig. 9.** The ipRGCs in mouse CMZ appear negative for the transcription factor Brn3b. The CMZ from nasal (A and B) and temporal (C) retina largely contains Brn3b negative ipRGCs, with occasional examples of low-level Brn3b expression (green) in the more weakly stained melanopsin cells (red). The green channel is separated below each image in A–C, where the arrows correspond to ipRGC somas highlighted by arrows in the merged image above. Note that the positive Brn3b staining is apparent in surrounding nuclei (stars), while the intensely stained fluorescent green clumps are non-specific staining artefacts. Scale bar, 50  $\mu\text{m}$ . (For interpretation of the references to colour in this figure legend, the reader is referred to the web version of this article.)

had not previously noted retino-ciliary projections in the peripheral rat retina but a more detailed analysis of this region may reveal similar structures in the CMZ of rat. Interestingly, a recent detailed anatomical study of ipRGC distributions in mouse retina reported a non-uniform distribution of the different ipRGC subtypes but failed to detect the structure we describe here (Hughes et al., 2013). This most likely reflects the technical difficulty in preparing retinal whole mounts that include the CMZ.

The melanopsin-rich CMZ plexus and associated ipRGCs could survive axotomy and remain light-responsive *in vivo* for up to 2-months post-axotomy. As such these cells had the potential to contribute to the robust *in vivo* iPLR we observed in bilaterally axotomised mice. However, melanopsin staining in the CMZ plexus appeared much less intense in the axotomised animals compared to wildtype mice (compare Fig. 4 with Figs. 6–9).

The sparse retino-ciliary projections we observed in pigmented wildtype mice appear to originate from small, Brn3b negative M1-type ipRGCs and may represent the start of axonal processes, which ramify further in ciliary body and/or iris. This would make sense as melanopsin expression stops at the optic nerve head in rodents, while melanopsin-negative ipRGC axons extend to innervate sub-cortical targets in the brain (Hattar et al., 2002). Also, it is known

that M1 cell axons in the mouse retina send collaterals up towards unexpected retinal locations (Joo et al., 2013). During the preparation of this manuscript we became aware of a report at the annual ARVO meeting detailing the use of transgenic reporter mice to visualise axons of ipRGC origin in the iris of albino mice (Rupp et al., 2013). This abstract also reported data supportive of a role for neurotransmission in the production of iPLR and suggested that the ipsilateral iPLR is driven by the 200 Brn3b negative M1 ipRGCs which can also mediate circadian photoentrainment (Chen et al., 2011). Our finding of Brn3b negative ipRGCs in the melanopsin-rich CMZ plexus of mice supports this hypothesis and together with data from the study by Chen and colleagues which shows  $\sim 50\%$  constriction to intense light in mice containing only Brn3b negative ipRGCs ( $5.66 \text{ mW/cm}^2$ ).

In addition to the melanopsin-rich CMZ plexus and occasional retino-ciliary projections we also report that melanopsin is expressed at low levels in the ciliary body itself. This is not unexpected, because Xue and colleagues had already noted that melanopsin immunoreactivity in mouse iris was not confined to the sphincter muscle. Therefore, it is possible that light causes constriction of ciliary body independent of iris sphincter and ipRGC signalling. Constriction of the ciliary body leads to accommodation, a process involving changes in the curvature of the lens and pupillary constriction (Alexandridis, 1985). It is therefore possible that melanopsin mediated phototransduction in the ciliary body may contribute to focussing near objects under bright lighting conditions by altering the shape of the lens. Aside from a potential role in the iPLR, it is important to note that our finding of melanopsin expression in cells of the ciliary body also has relevance to retinal stem cell research, with substantial efforts over recent years directed to identifying and expanding retinal progenitor cells from either the ciliary body or CMZ (Bhatia et al., 2010; Moshiri and Reh, 2004; Tropepe et al., 2000). Our findings suggest that cells isolated from the ciliary body of mice may already be intrinsically light responsive and given the emerging role for ipRGCs in early retinal development (Renna et al., 2011), the melanopsin-rich nasal plexus we report suggests the potential for temporal-nasal variation in the potential to derive progenitor cells from the CMZ of mice.

In terms of the functional significance of iPLR for mice, the response may obviously help to maintain pupillary constriction under constant illumination. However, melanopsin signalling in the iris could also be important for signalling ocular discomfort in response to very bright light, as indicated by the sharp increase in magnitude of iPLR we detect between  $630 \mu\text{W/cm}^2$  and  $6.3 \text{ mW/cm}^2$ . Such a function may help rodents to avoid danger in open, brightly lit spaces.

Recent work has shown that light can trigger trigeminal nerve activity in axotomised rats (Dolgonos et al., 2011) and given the association between melanopsin signalling and light aversion behaviour/photophobia (Noseda et al., 2010; Semo et al., 2010), we suggest that melanopsin signalling in the iris may well lead to trigeminal signalling independent of the brain in rodents. This possibility may also be important to consider when interpreting melanopsin-driven cortical activation data in rodents (Brown et al., 2010). This work by Brown and colleagues shows a slow activation of retrosplenial cortex and V2 in *rd/rd cl* mice, which could in part result from iridial melanopsin signalling activating the extended visual cortex independently of optic nerve via the trigeminal nerve and dura/light-sensitive thalamic relay neurons (Noseda et al., 2010).

## 5. Conclusions

Previous work in mice has identified a requirement for melanopsin and the beta subunit of phospholipase C in the light-

induced tension responses of isolated iris sphincter muscle (Xue et al., 2011). The findings of the present study extend our understanding of this melanopsin-dependent iPLR to reveal that it is composed of at least 2 components, one involving constriction of the iris sphincter muscle and another involving signalling at the ciliary body/CMZ. The iPLR response is sensitive to blockade of cholinergic neurotransmission and may involve direct communication between ipRGCs in the retina and post-synaptic sites in the iris. Although we cannot presently rule out a role for rods/cones in any retinal component of the iPLR in wildtype mice, we consider this possibility unlikely. Given that acetylcholine is known to cause relaxation of the iris dilator muscle (Suzuki et al., 1983), we propose that melanopsin-driven constriction of the iris sphincter is augmented by an ipRGC-driven, cholinergic-dependent relaxation of the iris dilator muscle. Additional components of the iPLR response may involve direct light-mediated contraction of the ciliary body (present study) and an ipRGC-driven, cholinergic-dependent constriction of the iris sphincter muscle (Rupp et al., 2013).

### Acknowledgements

This work was funded by an UCL-Institute of Ophthalmology discretionary grant and new lecturer award from the UK Charity fight for sight (AV). We would also like to thank Prof. Robert Lucas from the University of Manchester for the MKO mice and Prof. Peter Coffey from UCL-Institute of Ophthalmology for his continued support and use of equipment throughout the project.

### References

- Alexandridis, E., 1985. *Die Pupille: Physiologie-untersuchung-pathologie*. Springer-Verlag, New York.
- Barr, L., Alpern, M., 1963. Photosensitivity of the frog iris. *J. Gen. Physiol.* 46, 1249–1265.
- Berson, D.M., Dunn, F.A., Takao, M., 2002. Phototransduction by retinal ganglion cells that set the circadian clock. *Science* 295, 1070–1073.
- Bhatia, B., Singhal, S., Jayaram, H., Khaw, P.T., Limb, G.A., 2010. Adult retinal stem cells revisited. *Open Ophthalmol. J.* 4, 30–38.
- Bito, L.Z., Turansky, D.G., 1975. Photoactivation of pupillary constriction in the isolated in vitro iris of a mammal (*Mesocricetus auratus*). *Comp. Biochem. Physiol. A, Comp. Physiol.* 50, 407–413.
- Brown, T.M., Gias, C., Hatori, M., Keding, S.R., Semo, M., Coffey, P.J., Gigg, J., Piggins, H.D., Panda, S., Lucas, R.J., 2010. Melanopsin contributions to irradiance coding in the thalamo-cortical visual system. *PLoS Biol.* 8, e1000558.
- Chen, S.K., Badea, T.C., Hattar, S., 2011. Photoentrainment and pupillary light reflex are mediated by distinct populations of ipRGCs. *Nature* 476, 92–95.
- Dolgonos, S., Ayyala, H., Evinger, C., 2011. Light-induced trigeminal sensitization without central visual pathways: another mechanism for photophobia. *Invest. Ophthalmol. Vis. Sci.* 52, 7852–7858.
- Ecker, J.L., Dumitrescu, O.N., Wong, K.Y., Alam, N.M., Chen, S.K., Legates, T., Renna, J.M., Prusky, G.T., Berson, D.M., Hattar, S., 2010. Melanopsin-expressing retinal ganglion-cell photoreceptors: cellular diversity and role in pattern vision. *Neuron* 67, 49–60.
- Freedman, M.S., Lucas, R.J., Soni, B., von Schantz, M., Munoz, M., David-Gray, Z., Foster, R., 1999. Regulation of mammalian circadian behavior by non-rod, non-cone, ocular photoreceptors. *Science* 284, 502–504.
- Guler, A.D., Ecker, J.L., Lall, G.S., Haq, S., Altimus, C.M., Liao, H.W., Barnard, A.R., Cahill, H., Badea, T.C., Zhao, H., Hankins, M.W., Berson, D.M., Lucas, R.J., Yau, K.W., Hattar, S., 2008. Melanopsin cells are the principal conduits for rod-cone input to non-image-forming vision. *Nature* 453, 102–105.
- Hasan, S.M., Vugler, A.A., Miljan, E.A., Sinden, J.D., Moss, S.E., Greenwood, J., 2010. Immortalised human foetal retinal cells retain progenitor characteristics and represent a potential source for the treatment of retinal degenerative disease. *Cell Transpl.* 19, 1291–1306.
- Hattar, S., Liao, H.W., Takao, M., Berson, D.M., Yau, K.W., 2002. Melanopsin-containing retinal ganglion cells: architecture, projections, and intrinsic photosensitivity. *Science* 295, 1065–1070.
- Hughes, S., Watson, T.S., Foster, R.G., Peirson, S.N., Hankins, M.W., 2013. Nonuniform distribution and spectral tuning of photosensitive retinal ganglion cells of the mouse retina. *Curr. Biol.* 23, 1696–1701.
- Joo, H.R., Peterson, B.B., Dacey, D.M., Hattar, S., Chen, S.K., 2013. Recurrent axon collaterals of intrinsically photosensitive retinal ganglion cells. *Vis. Neurosci.* 30, 175–182.
- Kuder, T., 1986. The ciliary ganglion in mouse. *Folia Morphol.* 45, 80–85.
- Lau, K.C., So, K.F., Campbell, G., Lieberman, A.R., 1992. Pupillary constriction in response to light in rodents, which does not depend on central neural pathways. *J. Neurol. Sci.* 113, 70–79.
- Lucas, R.J., Douglas, R.H., Foster, R.G., 2001. Characterization of an ocular photopigment capable of driving pupillary constriction in mice. *Nat. Neurosci.* 4, 621–626.
- Lucas, R.J., Hattar, S., Takao, M., Berson, D.M., Foster, R.G., Yau, K.W., 2003. Diminished pupillary light reflex at high irradiances in melanopsin-knockout mice. *Science* 299, 245–247.
- May, C.A., Lutjen-Drecoll, E., 2002. Morphology of the murine optic nerve. *Invest. Ophthalmol. Vis. Sci.* 43, 2206–2212.
- Moshiri, A., Reh, T.A., 2004. Persistent progenitors at the retinal margin of ptc+/- mice. *J. Neurosci.* 24, 229–237.
- Nosedá, R., Kainz, V., Jakubowski, M., Gooley, J.J., Saper, C.B., Digre, K., Burstein, R., 2010. A neural mechanism for exacerbation of headache by light. *Nat. Neurosci.* 13, 239–245.
- Nowak, E., Kuder, T., Szczyrkowski, A., Kuchinka, J., 2004. Anatomical and histological data on the ciliary ganglion in the Egyptian spiny mouse (*Acomys cahirinus* Desmarest). *Folia Morphol.* 63, 267–272.
- Provencio, I., Rollag, M.D., Castrucci, A.M., 2002. Photoreceptive net in the mammalian retina. This mesh of cells may explain how some blind mice can still tell day from night. *Nature* 415, 493.
- Renna, J.M., Weng, S., Berson, D.M., 2011. Light acts through melanopsin to alter retinal waves and segregation of retinogeniculate afferents. *Nat. Neurosci.* 14, 827–829.
- Rupp, A., Schmidt, T., Chew, K., Yungheer, B., Park, K., Hattar, S., 2013. ipRGCs mediate ipsilateral pupil constriction. In: *ARVO Annual Meeting Abstract*, p. 310.
- Schmidt, T.M., Chen, S.K., Hattar, S., 2011. Intrinsically photosensitive retinal ganglion cells: many subtypes, diverse functions. *Trends Neurosci.* 34, 572–580.
- Seliger, H.H., 1962. Direct action of light in naturally pigmented muscle fibers. I. Action spectrum for contraction in eel iris sphincter. *J. Gen. Physiol.* 46, 333–342.
- Semo, M., Gias, C., Ahmado, A., Sugano, E., Allen, A.E., Lawrence, J.M., Tomita, H., Coffey, P.J., Vugler, A.A., 2010. Dissecting a role for melanopsin in behavioural light aversion reveals a response independent of conventional photoreception. *PLoS ONE* 5, e15009.
- Semo, M., Lupi, D., Peirson, S.N., Butler, J.N., Foster, R.G., 2003. Light-induced c-fos in melanopsin retinal ganglion cells of young and aged rodless/coneless (rd/rd cl) mice. *Eur. J. Neurosci.* 18, 3007–3017.
- Smith, R.S., Sundberg, J.P., Simon, W.M.J., 2002. The anterior segment and ocular adnexae. In: Smith, R. (Ed.), *Systematic Evaluation of the Mouse Eye: Anatomy, Pathology, and Biomethods*. CRC Press LLC, Boca Raton, Florida, pp. 13–15.
- Suzuki, R., Oso, T., Kobayashi, S., 1983. Cholinergic inhibitory response in the bovine iris dilator muscle. *Invest. Ophthalmol. Vis. Sci.* 24, 760–765.
- Tropepe, V., Coles, B.L., Chiasson, B.J., Horsford, D.J., Elia, A.J., McInnes, R.R., van der Kooy, D., 2000. Retinal stem cells in the adult mammalian eye. *Science* 287, 2032–2036.
- Tu, D.C., Batten, M.L., Palczewski, K., Van Gelder, R.N., 2004. Nonvisual photoreception in the chick iris. *Science* 306, 129–131.
- Vugler, A.A., Coffey, P.J., 2003. Loss of calretinin immunoreactive fibers in subcortical visual recipient structures of the RCS dystrophic rat. *Exp. Neurol.* 184, 464–478.
- Vugler, A.A., Semo, M., Joseph, A., Jeffery, G., 2008. Survival and remodeling of melanopsin cells during retinal dystrophy. *Vis. Neurosci.* 25, 125–138.
- Xue, T., Do, M.T., Riccio, A., Jiang, Z., Hsieh, J., Wang, H.C., Merbs, S.L., Welsbie, D.S., Yoshioka, T., Weissgerber, P., Stolz, S., Flockerzi, V., Freichel, M., Simon, M.J., Clapham, D.E., Yau, K.W., 2011. Melanopsin signalling in mammalian iris and retina. *Nature* 479, 67–73.